

New determination of the asymptotic D -state to S -state ratio of the triton using (\vec{d}, t) reactions at sub-Coulomb energies

E. A. George and L. D. Knutson

Physics Department, University of Wisconsin-Madison, Madison, Wisconsin 53706

(Received 14 April 1993)

The asymptotic D -state to S -state ratio of the ${}^3\text{H} \rightarrow n + d$ cluster wave function (η_t) has been determined from measurements of sub-Coulomb (\vec{d}, t) tensor analyzing powers. New measurements of the tensor analyzing power T_{20} for (\vec{d}, t) reactions on ${}^{208}\text{Pb}$ and ${}^{119}\text{Sn}$ at several different energies are presented. These data, along with previous measurements of T_{20} and T_{21} for several additional reactions and energies, are used in a distorted-wave Born approximation analysis that includes nuclear tensor potentials as well as long-range tensor potentials that arise from Coulomb interactions. A weighted mean of all 14 statistically independent values gives the result $\eta_t = -0.0431 \pm 0.0025$, where the quoted uncertainty includes statistical and systematic contributions. This result is compared with previous measurements and with predictions obtained from Faddeev calculations.

PACS number(s): 21.45.+v, 24.50.+g, 25.45.Hi, 27.10.+h

I. INTRODUCTION

At the present time, there is a great deal of interest in understanding the spin structure of light nuclei, particularly of the $A = 3$ nuclei, ${}^3\text{H}$ and ${}^3\text{He}$. These nuclei represent an important testing ground for models of the NN interaction and for studies of the many-body aspects of the strong interaction in nuclei. One reason for this importance is that in the $3N$ system it is possible to carry out quantum-mechanical calculations that are essentially exact. In addition, this is the simplest system in which the effects of possible three-body nuclear forces can be explored. Also, we note that there are a number of experiments currently being planned (for example, experiments to study the scattering of electrons from the polarized neutron within a polarized ${}^3\text{He}$ nucleus) that rely on a detailed knowledge of the spin structure of the bound-state wave functions of $A = 3$ nuclei.

The new work reported in this paper concerns the properties of the D -state component of the ${}^3\text{H}$ wave function. The existence of this D -state component, which arises fundamentally from the NN tensor force, has been understood theoretically for 50 years. The D -state wave function is complex in form, with several distinct configurations allowed by parity and angular momentum conservation. Modern Faddeev calculations employing realistic NN interactions predict D -state probabilities in the neighborhood of 9%.

Unfortunately, direct experimental information concerning the nature of the D -state components of the $A = 3$ nuclei is relatively scarce, and what information there is is generally not of high accuracy. The only quantity directly associated with the ${}^3\text{H}$ D state that can be reliably determined at the present time is the asymptotic D -state to S -state ratio of the ${}^3\text{H} \rightarrow n + d$ cluster wave function, η_t . Measurements of this quantity are clearly of importance since they provide a means for testing the theoretical wave functions obtained by direct solution of

the Faddeev equations. In addition to the general interest in obtaining experimental results that relate to the spin structure of ${}^3\text{H}$, there has recently been renewed interest in determinations of η_t , stimulated in part by theoretical work that has provided a clear prediction for this quantity. Until recently, however, η_t had been determined experimentally to only 10–20%.

In this paper, we describe recent experimental work that has led to a new determination of η_t . This new determination is obtained by comparing measurements of the tensor analyzing powers for sub-Coulomb (\vec{d}, t) reactions with distorted-wave Born approximation (DWBA) calculations of those analyzing powers. Our data set includes previously reported [1, 2] measurements of the tensor analyzing powers T_{20} and T_{21} for five different (\vec{d}, t) reactions, as well as new measurements of T_{20} for several reactions at lower energy and with higher precision than the old data. Our determination is based on a data set that is more extensive and includes measurements at lower energy (and is therefore less sensitive to uncertainties in the calculations) than for any previous determination of η_t by this method.

In Sec. II, we discuss the background information which is relevant to this determination of η_t . Section III contains a description of the experimental details for the new analyzing power measurements. The DWBA analysis of the measurements is discussed in Sec. IV. Results are presented in Sec. V, and are discussed and compared to previous theoretical and experimental determinations in Sec. VI.

II. BACKGROUND

A. Previous determinations of η_t

At this time, there are clear theoretical predictions for η_t [3–5]. These predictions are based on the observation

that if one does many different Faddeev calculations of triton observables (using different two- and three-nucleon potentials and different numbers of channels), there is a linear correlation between η_t and the triton binding energy E_t [3, 4], and also between η_t/η_d and E_t [5]. If this linear correlation is evaluated at the experimentally determined value of the binding energy, $E_t = -8.48$ MeV, a prediction for η_t is obtained. The results from Refs. [3–5], which are listed in Table I, are reasonably consistent, differing from the average value, $\eta_t = -0.044$, by no more than 5%. Because these predictions are based on general principles and are so consistent, experimental tests of them are of immediate interest.

Previous experimental determinations of η_t fall into one of two categories: those obtained from extrapolation in angle of ${}^2\text{H}(\vec{d}, p){}^3\text{H}$ or ${}^4\text{He}(\vec{d}, {}^3\text{He}){}^3\text{H}$ spin observables to the neutron exchange pole (for example, Refs. [6–8]), and those obtained from distorted-wave Born approximation (DWBA) analysis of tensor analyzing powers for (\vec{d}, t) reactions, usually on heavy nuclei (for example, Refs. [1, 2, 9–11]). The first method (pole extrapolation) relies on the fact that tensor analyzing powers for reactions that involve the ${}^3\text{H} \rightarrow n + d$ vertex depend in a simple way on the triton asymptotic normalization constants at the neutron exchange pole. For physical values of the incident deuteron energy, the neutron exchange pole is at unphysical angles. Therefore, what is done is to fit the measured observables in the physical region with some function and use that function to extrapolate to the pole. One of the most difficult and controversial aspects of this method is the treatment of the systematic errors in the extrapolation procedure (see Refs. [8, 12, 13]).

Values for η_t obtained by this pole extrapolation method are given in Table I. The authors claim that the quoted errors include the effect of uncertainties in the extrapolation procedure, although this claim has not been independently verified. These results for η_t are consistent with the theoretical predictions at the one-standard-deviation level, but the uncertainties in these

experimental determinations are somewhat large.

The second method for determining η_t is based on the comparison of tensor analyzing powers for (\vec{d}, t) reactions to DWBA calculations. In early experiments of this type, the DWBA calculations were carried out using the local energy approximation (LEA) [14]. In the LEA, the D -state parameter that is determined is D_2 , which is approximately related to η_t by $D_2 \approx \eta_t/\alpha^2$, where

$$\alpha^2 = \frac{2m_d m_n (E_t - E_d)}{(m_d + m_n)\hbar^2}. \quad (1)$$

Karban and Tostevin [9] analyzed tensor analyzing power measurements for five different (\vec{d}, t) reactions on heavy nuclei and obtained $D_2 = -0.22 \pm 0.02$ (corresponding to $\eta_t = -0.044 \pm 0.004$). This was the first such analysis to include tensor potentials in the deuteron channel. More recent determinations are based on full finite-range DWBA calculations. These experiments determine η_t directly. For example, Bhat *et al.* [10] obtained a value for η_t of -0.050 ± 0.010 by comparing full finite-range DWBA calculations including deuteron tensor potentials with analyzing powers measured for ${}^{31}\text{P}(\vec{d}, t){}^{30}\text{P}$ at 16 MeV (see Table I). Uncertainties in the l -mixing amplitudes and in the optical model parameters used in the calculations are significant sources of uncertainty in this result.

If deuteron energies below the Coulomb barrier are used, the sensitivity to the optical model potentials is greatly reduced. Also, at low energy the tensor analyzing powers are, to a very good approximation, proportional to η_t . The calculated tensor analyzing powers are still somewhat dependent on the optical model potentials used in the calculation, especially on the deuteron-nucleus tensor potentials. It is important to estimate this contribution to the uncertainty carefully, since it can be significant, especially at energies not far below the Coulomb barrier.

The most recent value for η_t obtained from the DWBA analysis of sub-Coulomb tensor analyzing power data [11] is given in Table I. The tensor analyzing power data used for this determination were from three different (\vec{d}, t) reactions at deuteron energies ranging from 85% to 115% of the Coulomb barrier. (We take the Coulomb barrier to be the maximum height of the Coulomb potential plus the real part of the nuclear central potential, using the deuteron-nucleus optical model potential of Daehnick [15].) We believe [16] that the uncertainty in the result reported in Ref. [11] has been underestimated by a factor of 2 due to an underestimation of the error arising from the optical model potentials. The authors of Ref. [11] neglect the error arising from the uncertainty in the nuclear tensor potentials, whereas we find this to be the dominant error contribution. Even with the increased error, however, this determination of η_t is more precise than any previous determination and is consistent with the theoretical predictions.

B. Present determination

We have made a new determination of η_t using an extensive set of (\vec{d}, t) tensor analyzing power measurements.

TABLE I. Theoretical and experimental determinations of η_t .

Method	η_t	Reference
Theory		
Correlation of η_t and E_t	-0.0432(15)	[3]
Correlation of η_t and E_t	-0.046(1)	[4]
Correlation of η_t/η_d and E_t	-0.0430(12) ^a	[5]
Experiment		
Pole extrapolation, ${}^2\text{H}(\vec{d}, p){}^3\text{H}$	-0.048(7)	[6]
Pole extrapolation, ${}^2\text{H}(\vec{d}, p){}^3\text{H}$	-0.051(5)	[7]
Pole extrapolation, ${}^4\text{He}(\vec{d}, {}^3\text{He}){}^3\text{H}$	-0.050(6)	[8]
LEA DWBA analysis	-0.044(4)	[9]
DWBA analysis, ${}^{31}\text{P}(\vec{d}, t){}^{30}\text{P}$	-0.050(10)	[10]
Sub-Coulomb DWBA analysis	-0.043(4) ^b	[11]
This experiment	-0.0431(25)	—

^a Using $\eta_d = 0.0256(4)$ (Ref. [29]).

^b Uncertainty from Ref. [16].

Some of the measurements we use [1, 2] were obtained at our laboratory about ten years ago for use as part of a similar, but less sophisticated, study of the triton D state. We have also obtained new data, making use of the increased beam current and fast polarization switching capability of our ion source [17] and an improved calibration of our deuteron polarimeter [18] to obtain more precise data, and data at lower energy, than was possible ten years ago. The deuteron energy of the data used in this determination of η_t ranges from 69% to 95% of the height of the Coulomb barrier. The lower energy (compared to Ref. [11]), plus the fact that our data set is more extensive (nine different energy, target, and final state combinations, compared to four for Ref. [11]), means that the present determination of η_t represents a significant improvement over previous work.

Our analysis is based on a full finite-range DWBA calculation, including nuclear tensor potentials. We also include the effects of long-range tensor potentials due to the Coulomb interaction of the deuteron and target nucleus. A significant part of the analysis is devoted to the estimation of the uncertainty in the result, especially the calculational uncertainties.

III. DESCRIPTION OF THE EXPERIMENT

We have measured the tensor analyzing power T_{20} [19] of the $^{119}\text{Sn}(\vec{d}, t)^{118}\text{Sn}$ reaction at 6.0 and 4.9 MeV, and of the $^{208}\text{Pb}(\vec{d}, t)^{207}\text{Pb}(E_x = 0.00, 0.57, 0.90 \text{ MeV})$ reactions at 9.0 MeV. We have also measured T_{20} for the $^{119}\text{Sn}(\vec{d}, t)^{118}\text{Sn}$ reaction at higher energies (7.0, 8.0, and 9.0 MeV) in order to determine the energy dependence of the tensor analyzing powers and to test the method of determining the uncertainty in the DWBA calculations.

The measurements were made at the University of Wisconsin tandem accelerator laboratory, using the deuteron beam from the crossed-beam polarized ion source [17]. The spin alignment axis of the beam was along the beam momentum direction so that the t_{20} beam moment was maximized, while the other components of the beam polarization were kept close to zero. The sign of the beam polarization was cycled between positive, negative, and unpolarized states at intervals of less than 1 sec. A polarimeter [18] located at the exit of the main scattering chamber was used to monitor continuously all relevant components of the beam polarization.

Beam-defining slits 1 mm high by 1.5 mm wide were placed at the entrance to the chamber. A tantalum antiscattering slit 3.2 mm in diameter was used to intercept deuterons that scattered off the edges of the beam-defining slits. The targets were enriched self-supporting foils. The ^{208}Pb target was isotopically enriched to 99.86% and was 1.01 mg/cm² thick. The ^{119}Sn targets were enriched to 85.9%; the target thickness was 1.65 mg/cm² for the 4.9 MeV measurements, and 2.62 mg/cm² for the other measurements. Reaction products were detected in three ΔE - E telescopes placed on the beam left side of the main scattering chamber, 10 cm from the target. The telescopes consisted of rectangular silicon surface-barrier detectors. The ΔE detectors

were 60 μm thick for the 4.9, 6.0, and 7.0 MeV ^{119}Sn measurements and 100 μm thick for the rest of the measurements. The E detectors were 2500–3000 μm thick. Rectangular slits 15.9 mm high by 3.2 mm wide defined detector solid angles of 4.9 msr.

Signals from the ΔE and E detectors of each telescope were processed separately, and then fed into two ADC's which were operated in coincidence mode. The ΔE and E signals were stored in a two-dimensional histogram, so that the difference in energy loss in the ΔE detector could be used to identify protons, deuterons, and tritons in the spectrum.

A sample ΔE - E spectrum for the $^{208}\text{Pb}(\vec{d}, t)^{207}\text{Pb}$ reaction is shown in Fig. 1(a). The three peaks seen in this spectrum correspond to tritons from reactions populating the ^{207}Pb final states at $E_x = 0.00, 0.57, \text{ and } 0.90$ MeV. The counts in the lower left corner of this spec-

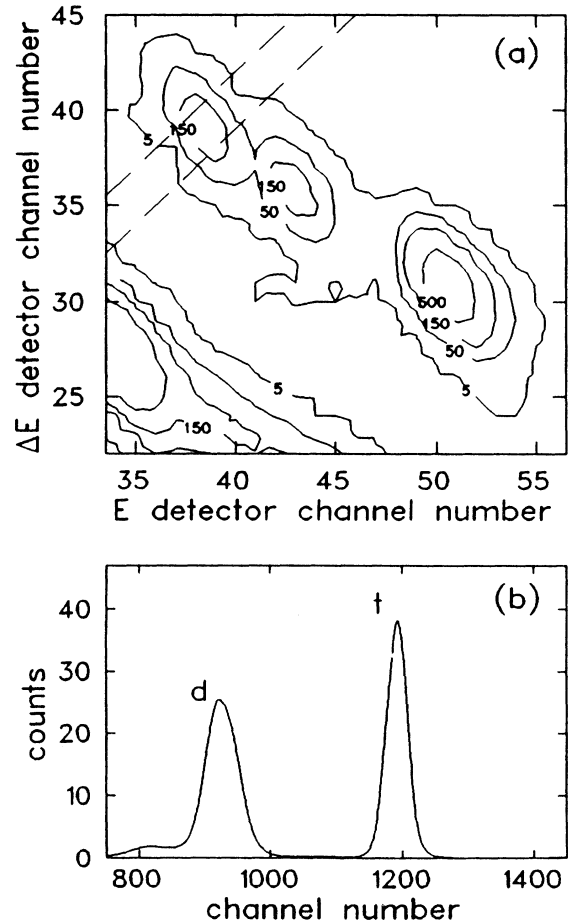


FIG. 1. Sample spectrum for the $^{208}\text{Pb}(\vec{d}, t)^{207}\text{Pb}$ reaction at $E_d = 9.0$ MeV and a laboratory angle of 160° . In (a), a two-dimensional ΔE - E spectrum is shown. The dashed lines show the limits used in producing the one-dimensional spectrum for the transition to the second excited state of ^{207}Pb . In (b) is shown the one-dimensional spectrum obtained from the two-dimensional spectrum by the method described in the text. This spectrum represents about 2 h of running time.

trum are from the low-energy tail of the d - ^{208}Pb elastic scattering peak and from deuteron elastic scattering from an ^{16}O contaminant in the target. We extract the triton peak sum by first projecting the region containing the triton peak onto a line perpendicular to the triton locus. The dashed line in Fig. 1(a) shows the region to be projected for the second excited state of ^{207}Pb . This results in a one-dimensional spectrum, as shown in Fig. 1(b). The background in the region of the triton peak is mostly due to pileup in the detectors and to the tail of the deuteron locus. The analyzing power of the background was statistically zero. The peak-to-background ratio was greater than 100 to 1 in all cases, except for the 4.9 MeV $^{119}\text{Sn}(d, t)^{118}\text{Sn}$ measurements (Fig. 2). In this case, the background was about 15% of the triton

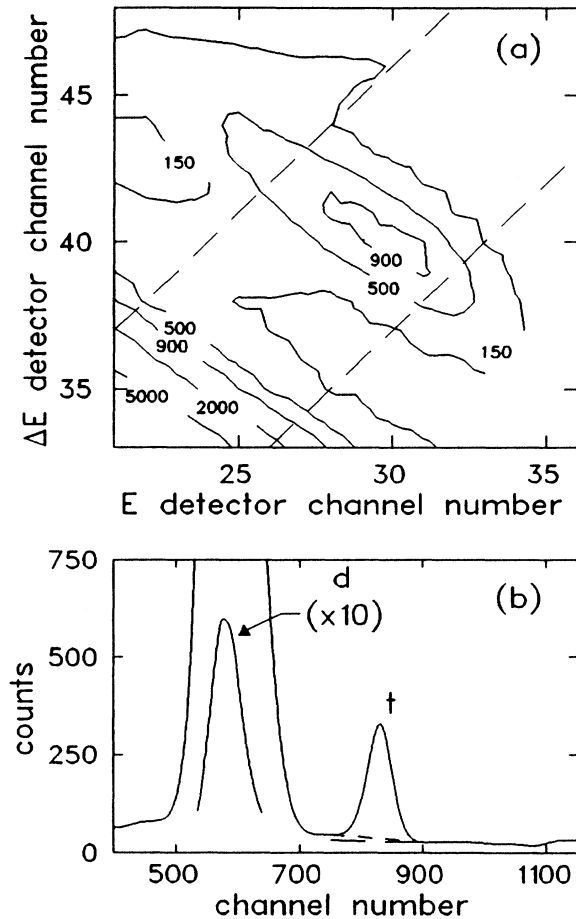


FIG. 2. Sample spectrum for the $^{119}\text{Sn}(d, t)^{118}\text{Sn}$ reaction at $E_d = 4.9$ MeV and a laboratory angle of 156° . In (a), a two-dimensional spectrum is shown. The dashed lines show the limits used in producing the one-dimensional spectrum. In (b) the one-dimensional spectrum is shown. The lines under the triton peak show the two methods of determining the background; the long dashes correspond to the linear extrapolation of the high-channel background only, while the short dashes correspond to a linear fit to the high- and low-channel background. This spectrum represents about 100 h of running time.

peak sum.

For the spectra in which the background was small, the contribution of the background to the peak was subtracted by determining the number of background counts in representative regions on both sides of the triton peak in the one-dimensional spectrum. The background was assumed to be linear. For each spectrum, several different choices of background regions were used so the uncertainty due to the choice of cuts could be estimated. The subtracted background was less than 2% of the total peak sum in all these cases, and the resulting fractional change in T_{20} was also less than 2%.

Because the background was so large for the 4.9 MeV ^{119}Sn data, the background subtraction was less straightforward. Peak fitting suggests that the deuteron peak does not extend under the relatively narrow window used for obtaining the triton peak sums. Therefore, the background was subtracted away by assuming that the background was linear, and that the region above the triton peak could be used to characterize the background. The region above the peak was fit with a line, which was then extrapolated back under the peak sum region to determine the background to be subtracted. The background correction obtained in this way ranged from 7% to 17% of the measured analyzing powers.

To obtain an estimate of the uncertainty in this correction, we subtracted away the background in a different way, by assuming a linear background and using regions on both sides of the peak to determine the background, just as was done for the rest of the data. As can be seen in Fig. 2(b), this method leads to larger background corrections. We believe the first method of background subtraction is probably more reasonable. The difference between the corrections obtained using the two different methods, however, gives a good estimate of the range of possibilities for the background correction. The uncertainty estimated in this way ranged from 2% to 7% of the measured analyzing powers, or about 40% of the correction itself. Because the background correction depends strongly on the method of background subtraction, and does so in the same way for each angle, the uncertainty in the background correction is correlated from angle to angle.

The analyzing power T_{20} was determined by using the expression

$$T_{20} = \frac{R - 1}{t_{20}^+ - R t_{20}^-}, \quad (2)$$

where $R = F^+/F^-$. The quantities F^+ and F^- represent the number of counts divided by the integrated charge in the state with beam polarization t_{20}^+ and the state with beam polarization t_{20}^- , respectively. We used detectors on the left side of the beam only, so there is a small correction to T_{20} due to the small but nonzero t_{21} and t_{22} beam moments. The data analysis was initially done by assuming that the non- t_{20} beam moments are identically zero. A DWBA calculation that fits the T_{20} data was then used to determine values for T_{21} and T_{22} , and these calculated values were used with the measured beam moments to determine a correction to the T_{20} data. In all cases, this correction is less than 2% of

the measured analyzing powers.

The measured T_{20} analyzing powers are shown in Fig. 3, Fig. 4, and Fig. 5. The uncertainties shown in the figures include statistical errors in the peak sums, background sums, and beam moments; uncertainties in the correction for nonzero t_{21} and t_{22} beam moments; and uncertainties arising from the choice of the background and peak sum regions. In addition to the corrections for background and for nonzero off-axis beam moments, corrections were made for electronic dead time and for errors in integrated charge due to finite response time of the integrating circuit. All corrections were less than 2% of the measured analyzing powers, except the background correction for the ^{119}Sn data, which ranged from 7% to 17% of the measured analyzing powers, as mentioned before. The error bars shown in Fig. 4 for the 4.9 MeV ^{119}Sn analyzing powers do not include the uncertainty in the background correction. This is because the background correction at this energy is dominated by the systematic errors associated with the choice of background subtraction method, which means that the background errors are correlated from angle to angle. We will return to the effect of the background uncertainty in Sec. IV D, where

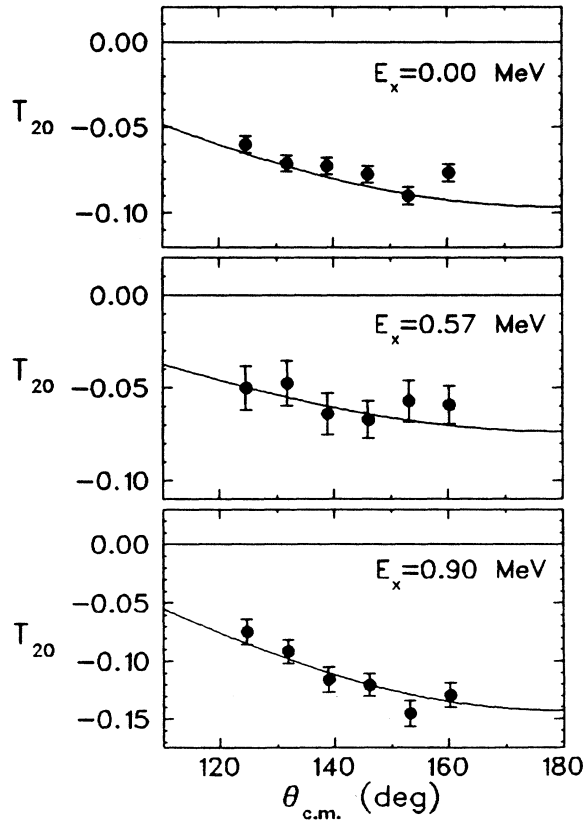


FIG. 3. Comparison of DWBA calculations with measured tensor analyzing powers T_{20} for $^{208}\text{Pb}(\vec{d},t)^{207}\text{Pb}$ at $E_d = 9.0$ MeV. The error bars include the statistical uncertainty and the uncertainty in the corrections for background and nonzero off-axis beam moments. The solid line is a DWBA calculation with $\eta_t = -0.043$.

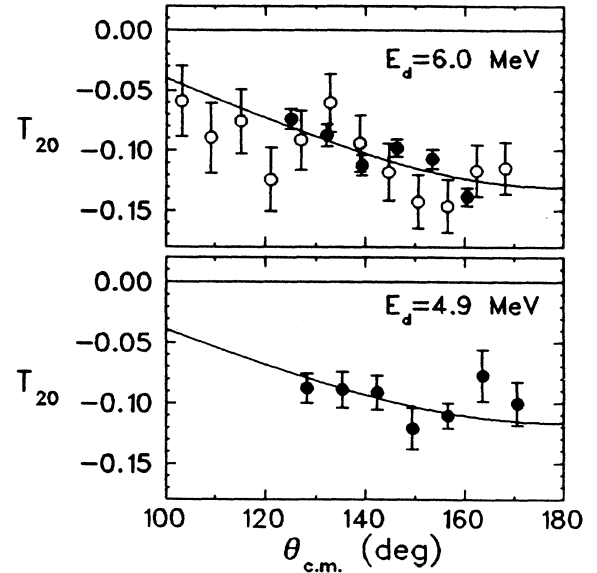


FIG. 4. Comparison of DWBA calculations with measured tensor analyzing powers T_{20} for $^{119}\text{Sn}(\vec{d},t)^{118}\text{Sn}$ at $E_d = 6.0$ and 4.9 MeV. The previously measured data at 6.0 MeV are shown as open circles. The comments of Fig. 3 apply.

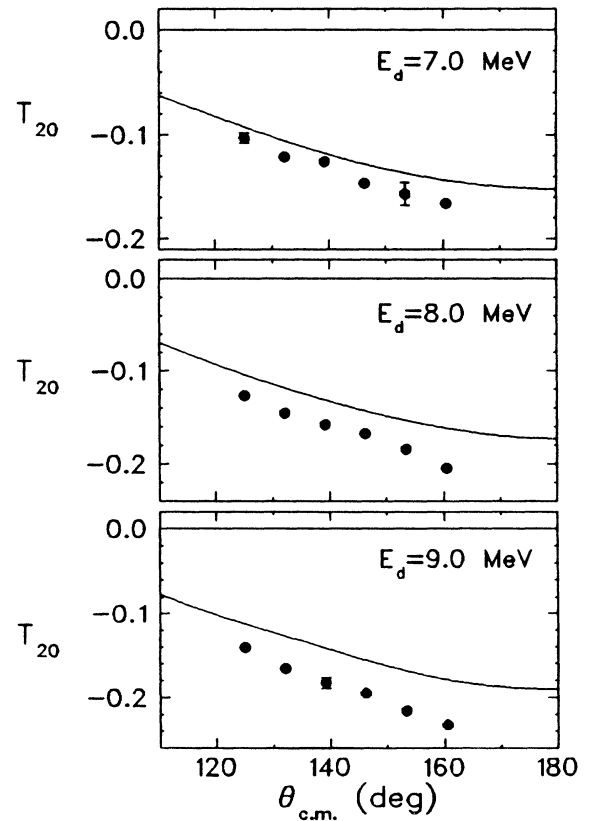


FIG. 5. Comparison of DWBA calculations with measured tensor analyzing powers T_{20} for $^{119}\text{Sn}(\vec{d},t)^{118}\text{Sn}$ at $E_d = 7.0, 8.0,$ and 9.0 MeV. The comments of Fig. 3 apply.

we discuss the determination of the uncertainty in η_t .

The old measurements of T_{20} for the $^{119}\text{Sn}(\vec{d}, t)^{118}\text{Sn}$ reaction at 6.0 MeV are shown along with the new measurements in Fig. 4. The old ^{119}Sn T_{20} data have been corrected for the recalibration of the polarimeter that was recently performed by Rodning [20]. These corrections were less than 2%.

IV. THE DWBA ANALYSIS

A. General considerations

For several reasons, DWBA calculations are expected to be very reliable for (d, t) reactions at sub-Coulomb energies [21]. Since the Coulomb barrier excludes the incident and outgoing particles from the region near the target nucleus, the nuclear potential has little effect on the reaction. Also, the incoming and outgoing distorted waves are nearly pure Coulomb waves, and are therefore known accurately.

The choice of bombarding energy has an important effect on the determination of η_t . At lower bombarding energies, the DWBA calculations are less sensitive to the nuclear potential, which means that the systematic errors from uncertainties in the calculations are smaller. This is important, since a large part of the uncertainty in the result comes from the uncertainties in the scattering and bound-state wave functions. On the other hand, the reaction cross section drops rapidly with energy; therefore, the experiments become more difficult and the statistical errors are larger at lower energies.

The specific reactions studied were chosen to reduce calculational uncertainties. Reactions with Q values near zero are advantageous, since in this case the incoming and outgoing scattering wave peak at nearly the same radial distance, enhancing the overlap and therefore reducing the contribution to the reaction amplitude from the region near the nucleus. If the angular momentum transferred by the neutron (j_n) is unique, there is no uncertainty in the calculation of the analyzing powers due to uncertainties in spectroscopic factors. All of the reactions in our data set have unique j_n . Most of the reactions have $j_n = l_n + 1/2$, since tensor analyzing powers for these transitions tend to be larger in magnitude than tensor analyzing powers for transitions with $j_n = l_n - 1/2$ (see Ref. [22]). In addition, the transitions chosen have fairly large spectroscopic factors to reduce the contributions to the reaction from multistep and collective processes. The target nuclei used have no low-lying collective states.

B. Details of the calculation

The DWBA calculations were performed using a version of the full finite-range program PTOLEMY [23] that has been modified to include spin degrees of freedom and to permit the use of tensor deuteron-nucleus potentials. This version of PTOLEMY has also been modified to be suitable for light-ion transfer reactions.

The central and spin-orbit parts of the optical potential in the deuteron channel were taken from Daehnick *et*

al. [15]. The optical potential in the triton channel was taken from Becchetti and Greenlees [24]. A measure of the sensitivity of the calculations to the choice of optical model potentials can be obtained by setting each of the potential depths to zero individually. For the 10 MeV $^{208}\text{Pb}(\vec{d}, t)^{207}\text{Pb}$ reactions (the reactions in our set most sensitive to the nuclear potentials) it was found that the real central and spin-orbit components do not have a significant effect (less than 2%) on the calculations. Turning off the absorptive potentials, however, produced a 10% or larger effect on the calculated tensor analyzing powers. Thus, except for the absorptive potentials, the particular central and spin-orbit potentials chosen have little effect on the calculated analyzing powers.

In addition to the central and spin-orbit terms, the potential also includes a nuclear tensor potential of the form

$$[V_{TR}(r) + iW_{TR}(r)]T_r, \quad (3)$$

where $T_r = (\mathbf{s} \cdot \hat{r})^2 - \frac{2}{3}$. The choice of tensor potentials can affect the calculated tensor analyzing powers significantly at the energies represented in our data set. The folding model predicts both real and imaginary parts to the tensor potential [25]. However, tensor analyzing power measurements for $^{208}\text{Pb}(\vec{d}, d)$ at 10.0 MeV [26], 9.0 MeV [27], and 8.0 MeV [28], for $^{90}\text{Zr}(\vec{d}, d)$ at 5.5 MeV [27], and for $^{136}\text{Xe}(\vec{d}, d)$ at 5.5 MeV [29] are not well reproduced by the folding model values. When used in conjunction with conventional central potentials, the full folding model tensor potential produces analyzing powers that are much larger in magnitude than the measurements. Reasonable agreement with the data can be achieved, however, by omitting either the real or the imaginary part of the potential, or by dividing both the real and the imaginary parts by a factor of 2 [except for the $^{90}\text{Zr}(\vec{d}, d)$ data, for which these calculated analyzing powers are still too large in magnitude]. In general, for any value of the real tensor potential between zero and the folding model value, a value for the imaginary tensor potential can be found that allows the elastic scattering data to be reproduced. We have chosen to use half the folding model strengths for the real and imaginary parts of the tensor potential for all reactions and energies in the data set. The effects of the uncertainty in the tensor potential are discussed in Sec. IV D.

In addition to the nuclear tensor potentials, we include two long-range tensor potentials that arise from Coulomb interactions between the deuteron and the target nucleus. The first,

$$V_{QT} = \frac{3}{2} Q Z e^2 r^{-3} T_r, \quad (4)$$

arises from the interaction of the deuteron quadrupole moment with the electric field gradient of the target nucleus. The strength and form of this potential are well known, since the interaction is purely electromagnetic and depends on the size of the deuteron quadrupole moment. The second long-range potential,

$$V_p = -\frac{1}{2} Z^2 e^2 r^{-4} (\alpha + 3\tau T_r), \quad (5)$$

is due to the electric polarization of the deuteron in the Coulomb field of the nucleus. This potential has a central part, which is proportional to α , and a tensor part, which is proportional to τ . The tensor part arises from the fact that the deuteron is more easily polarized when the electric field is along its spin alignment axis. The central term has a negligible effect on the analyzing powers, so we use only the tensor part of this potential in our calculation. We use the value $\tau = 0.0343 \text{ fm}^3$, calculated by Lopes *et al.* [30]. At the energies represented in our data set, including these two long-range potentials changes the calculated analyzing powers by a few percent of the analyzing powers.

The Coulomb field of the target nucleus produces electric polarization of the triton as well as the deuteron. These distortions can result in virtual P -state admixtures in the ${}^3\text{H} \rightarrow n + d$ cluster wave function. The effect of these P -state admixtures on the tensor analyzing powers has not been calculated, so we are not able to include these corrections in our results. For (\vec{d}, p) reactions, the contribution of virtual P states in the deuteron wave function to the tensor analyzing powers is approximately 2% [31]. One would expect the effect of P -state admixtures in the triton wave function on (\vec{d}, t) reactions to be somewhat less than this, because the triton is more tightly bound than the deuteron and also because the effect of the deuteron wave function on the analyzing powers is small [21].

The triton bound-state wave function used in the calculations was generated using the separation energy procedure. The potential used had a Woods-Saxon shape, with a radius parameter of $r = 1.5 \text{ fm}$ (corresponding to a radius of 1.89 fm) and $a = 0.5 \text{ fm}$ [10]; the potential depth was adjusted to reproduce the triton binding energy. The normalization of the S - and D -state components of the wave function was chosen to give $\eta_t = -0.04494$. We have chosen to use this wave function rather than a realistic one because its simple parametrization makes it easier to investigate the effect of uncertainties in the wave function on the calculations. We will discuss the adequacy of this choice of wave function in Sec. IV D.

The bound-state wave function of the picked-up neutron was generated in the same way as the triton wave function, with a real central potential of Woods-Saxon form with $r = 1.2 \text{ fm}$, $a = 0.7 \text{ fm}$. A real spin-orbit potential with $V_{\text{SO}} = 6.0 \text{ MeV}$ was also included.

C. Extracting a value for η_t

To extract a value of η_t from our analyzing power measurements, we use the fact that the calculated tensor analyzing powers are very nearly proportional to the value of η_t used in the DWBA calculation. Thus, we can find the value of η_t that gives the best fit to the data by minimizing

$$\chi^2 = \sum_i \left[\frac{(\eta_t/\eta_t^0)c_i - y_i}{\sigma_i} \right]^2. \quad (6)$$

Here, y_i are the measured analyzing powers with statistical uncertainties of σ_i . c_i are the analyzing powers calculated using a triton wave function with η_t^0 , which in our case was -0.04494 .

We have performed this minimization for all of the sub-Coulomb data. Results are listed in Table II, and are also represented graphically in Fig. 6. There are 14 statistically independent values of η_t . Values of the χ^2 per degree of freedom (χ_r^2) and confidence levels are also given in the table for each value. Generally speaking, the χ^2 values are acceptable, with the exception of the ${}^{147}\text{Sm } T_{20}$ measurements. This data set shows an unusual amount of scatter from angle to angle [2], and so large χ^2 values are inevitable.

The minimization was performed for the higher-energy (7, 8, and 9 MeV) ${}^{119}\text{Sn}$ data as well as for the sub-Coulomb data. We do not expect these higher-energy measurements to give an accurate result for η_t , primarily because of the greatly increased sensitivity of the calculations to details of the optical model potentials. Although these higher-energy (\vec{d}, t) data are not useful in determining the value of η_t , they do give us some insight into the error estimation procedure. We will return to this point

TABLE II. Values of η_t obtained from tensor analyzing power measurements for sub-Coulomb reactions.

Target	E_d (MeV)	E_x (MeV)	T_{kq}	η_t	χ_r^2	No. Pts.	C.L. (%)	$\Delta\eta_t^S$	$\Delta\eta_t^C$	$\Delta\eta_t^N$	Weight (%)
${}^{91}\text{Zr}$	5.0	0.00	T_{20}	-0.0392	1.74	12	6	0.0025	0.0023	0.0008	6.2
			T_{21}	-0.0459	0.89	12	54	0.0045	0.0021	0.0009	4.1
${}^{119}\text{Sn}$	6.0	0.00	T_{20}	-0.0430	1.30	18	18	0.0012	0.0028	0.0003	10.7
			T_{21}	-0.0519	0.92	12	52	0.0045	0.0029	0.0010	3.5
${}^{147}\text{Sm}$	4.9	0.00	T_{20}	-0.0427	0.86	6	52	0.0027	0.0014	0.0003	11.2
			T_{20}	-0.0468	2.64	8	1	0.0020	0.0016	0.0009	7.5
${}^{208}\text{Pb}$	10.0	0.00	T_{21}	-0.0495	1.43	8	19	0.0049	0.0016	0.0010	2.8
			T_{20}	-0.0384	1.06	12	39	0.0028	0.0042	0.0008	3.9
${}^{208}\text{Pb}$	9.0	0.00	T_{21}	-0.0413	1.22	12	26	0.0033	0.0035	0.0008	4.0
			T_{20}	-0.0426	0.61	12	82	0.0029	0.0028	0.0009	6.2
			T_{21}	-0.0457	0.94	12	50	0.0029	0.0023	0.0009	7.2
			T_{20}	-0.0398	1.31	6	26	0.0011	0.0026	0.0008	11.7
			T_{20}	-0.0404	0.38	6	86	0.0031	0.0032	0.0008	5.1
			T_{20}	-0.0432	0.84	6	52	0.0016	0.0018	0.0009	15.9

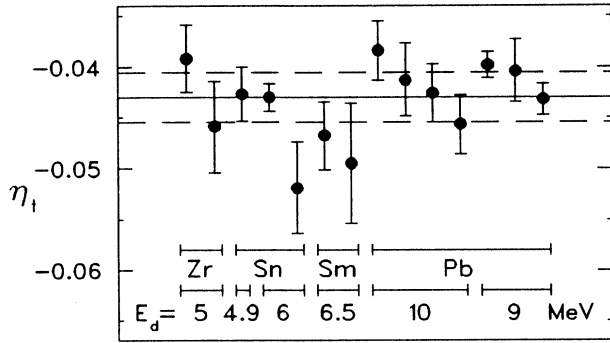


FIG. 6. Results for η_t for the 14 sub-Coulomb cases in Table II. The values are plotted in the order in which they are listed in the table. The error bars shown are the statistical error bars only; calculational and normalization uncertainties are not shown. The solid line represents the average of the individual values, weighted by the total uncertainty (statistical, calculational, and normalization) for each value. The dashed line represents the total error of the average.

in Sec. V. Results for these higher-energy measurements are given in Table III. Note that as the deuteron energy increases above the Coulomb barrier (which is about 7 MeV for deuterons on ^{119}Sn), the values of η_t determined from the data increase in magnitude.

D. Determination of the uncertainty

Systematic errors in the extraction of η_t can arise from uncertainties in the theoretical calculations of the (\vec{d}, t) tensor analyzing powers. The main contributions to this calculational error arise from uncertainties in the deuteron and triton elastic scattering wave functions (that is, in the optical model potentials) and to a lesser extent from uncertainties in the parameters used to specify the triton and bound-state neutron wave functions. We follow the method of Rodning and Knutson [29] to estimate the calculational uncertainty in η_t . First, we assign an uncertainty Δp_i to each parameter in the calculation. We then carry out DWBA calculations in which each parameter is varied individually by its uncertainty Δp_i in order to determine the sensitivity of the extracted value of η_t to that parameter ($\delta\eta_t/\delta p_i$). The net calculational uncertainty in η_t , $\Delta\eta_t^C$, is found by adding the contribution due to each of the parameters in quadrature:

$$\Delta\eta_t^C = \left[\sum_i \left(\frac{\delta\eta_t}{\delta p_i} \Delta p_i \right)^2 \right]^{1/2}. \quad (7)$$

The difficult part of this procedure is assigning uncertainties to the parameters. As in [29], we fix the radius and diffuseness parameters for all the potentials, and assign to the depth an uncertainty large enough to cover the uncertainty in the geometry parameters.

For the real central, absorptive, and spin-orbit potentials in the deuteron channel, we use uncertainties of $\pm 30\%$, based on the analysis of Ref. [29]. We also use uncertainties of $\pm 30\%$ in the potential depths in the triton channel, based on fits to $^{208}\text{Pb}(t, t)^{208}\text{Pb}$ cross section data at 9 MeV [32].

Another way to estimate the uncertainty due to the central and spin-orbit potentials is to repeat the DWBA calculations with different sets of optical model potentials, keeping the tensor potentials fixed at their original values. We did this for deuteron potentials from Daehnick *et al.* [15], Lohr [33], Lohr and Haeberli [34], Bojowald *et al.* [35], and Perrin *et al.* [36], and triton potentials from Becchetti and Greenlees [24], Hardekopf *et al.* [37], and Flynn *et al.* [38]. In this case, the uncertainty due to the central and spin-orbit potentials is taken to be the standard deviation of the set of resulting η_t values. For a given reaction, these uncertainties are up to three times larger than the uncertainties obtained from the method described in the previous paragraph. However, since the central and spin-orbit potentials contribute only a small amount to the total uncertainty for most of the reactions, the net effect on the final value of $\Delta\eta_t^C$ is small.

The largest contributions to $\Delta\eta_t^C$ arise from the deuteron-nucleus tensor potentials. Since a real or an imaginary potential, or a combination of both, could be used to fit the sub-Coulomb elastic scattering data, we choose uncertainties of $\pm 100\%$ for both the real and the imaginary parts of the tensor potential. This means that the real and imaginary depths are allowed to vary independently from zero to the folding model value.

The uncertainty arising from the long-range tensor potentials is also obtained in the same way as in [29]. The error due to the quadrupole tensor term is negligible, since the quadrupole moment of the deuteron is known to high precision. To calculate the error due to the tensor polarizability term, we assign an uncertainty of $\pm 10\%$ to the value of τ calculated by Lopes.

To determine the uncertainty due to the wave function used for the bound-state neutron in the target nucleus, we assign uncertainties of $\pm 15\%$ to the radius and diffuseness parameters. The spin-orbit potential depth in the neutron bound-state calculation was allowed to vary by $\pm 30\%$.

For the triton wave function, uncertainties of 20% in the radius and diffuseness parameters were used. This means, for example, that r is allowed to vary from 1.2 to 1.8 fm. The radial form factors $v_0(r)$ and $v_2(r)$ corresponding to these values of r are shown in Fig. 7. At the energies represented in our data set, the tensor analyzing powers depend mainly on the low-momentum behavior of the momentum-space form factors $v_L(k) =$

TABLE III. Values of η_t obtained from tensor analyzing power measurements for $^{119}\text{Sn}(\vec{d}, t)^{118}\text{Sn}$, with deuteron energies at or above the Coulomb barrier.

E_d (MeV)	η_t	χ_r^2	C.L. (%)	$\Delta\eta_t^S$	$\Delta\eta_t^C$	$\Delta\eta_t^N$
7.0	-0.0486	0.88	49	0.0007	0.0050	0.0010
8.0	-0.0522	0.94	45	0.0006	0.0073	0.0010
9.0	-0.0550	0.51	77	0.0006	0.0095	0.0011

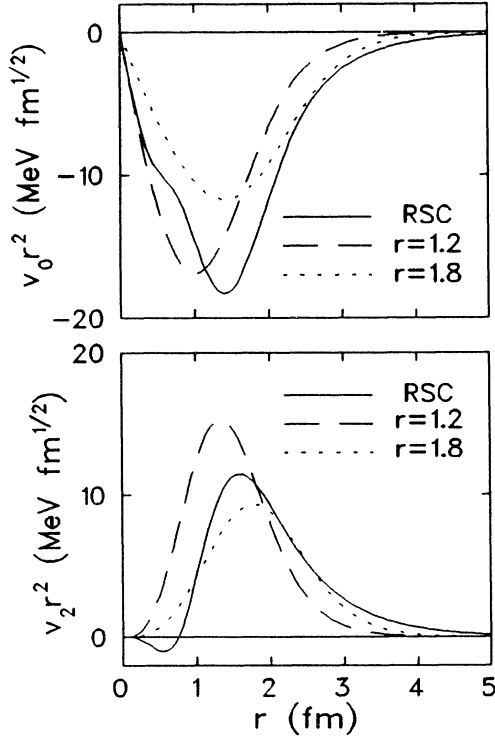


FIG. 7. Form factors multiplied by r^2 for the realistic triton wave function of Ref. [39] for the Reid soft-core potential (solid line), and for the wave function generated via the separation energy procedure using a Woods-Saxon potential with $r = 1.2$ fm, $a = 0.5$ fm (dashed line) and $r = 1.8$ fm, $a = 0.5$ fm (dotted line).

$\int_0^\infty j_L(kr) v_L(r) r^2 dr$. Therefore, in order to emphasize the regions that are important for low momenta, the radial form factors have been multiplied by r^2 . Also shown in Fig. 7 for comparison are the form factors for the Reid soft-core potential from the Faddeev calculation of Sasakawa and Sawada [39]. If the (\vec{d}, t) tensor analyzing powers do not depend only on the asymptotic D - to S -state ratio for the wave function, then the extracted η_t value may depend to some extent on the shape of the assumed form factors. Figure 7 demonstrates that the range of parameter values we employ, $r = 1.5 \pm 0.3$ fm and $a = 0.5 \pm 0.1$ fm, correspond to a wide range of form factor shapes, and that this range encompasses the Faddeev prediction.

The contributions to $\Delta\eta_t^C$ from all these individual parameters are shown in Table IV for the case of $^{208}\text{Pb}(\vec{d}, t)^{207}\text{Pb}(E_x = 0.90 \text{ MeV})$ at $E_d = 9.0 \text{ MeV}$. Most of $\Delta\eta_t^C$ comes from the uncertainty in the nuclear tensor potentials. This is typical of the results for all reactions and energies in our data set.

To produce a value for the net uncertainty due to the theoretical calculation, the contributions from the individual components are added in quadrature. This result is shown in Table II as $\Delta\eta_t^C$. An additional $\pm 2\%$ has been added in quadrature to $\Delta\eta_t^C$ to account for effects

TABLE IV. Contribution of individual parameters to the total calculational uncertainty for the reaction $^{208}\text{Pb}(\vec{d}, t)^{207}\text{Pb}(E_x = 0.90 \text{ MeV})$ at $E_d = 9 \text{ MeV}$.

Parameter (p_i)	Δp_i	$(\Delta\eta_t^C)_i$
$d + ^{208}\text{Pb}$		
Real V	$\pm 30\%$	< 0.0001
Surface imaginary V	$\pm 30\%$	0.0002
Spin-orbit V	$\pm 30\%$	< 0.0001
Real tensor V	$\pm 100\%$	0.0006
Imaginary tensor V	$\pm 100\%$	0.0013
Quadrupole tensor V	$\pm 0\%$	—
Polarization tensor V	$\pm 10\%$	0.0002
$t + ^{207}\text{Pb}$		
Real V	$\pm 30\%$	0.0001
Imaginary V	$\pm 30\%$	< 0.0001
Spin-orbit V	$\pm 30\%$	< 0.0001
Triton bound state r, a		
	$\pm 20\%$	0.0005
^{208}Pb bound state r, a		
	$\pm 15\%$	0.0002

that were not investigated, such as virtual P -state effects, effects of channel coupling, and so on. Also shown in Table II are the uncertainties arising from statistical uncertainty ($\Delta\eta_t^S$) and uncertainty in the overall normalization of the beam moments ($\Delta\eta_t^N$). An additional $\pm 3.5\%$ was added in quadrature to $\Delta\eta_t^S$ for the 4.9 MeV ^{119}Sn result to account for the possible systematic errors in the choice of background subtraction method discussed in Sec. III. The beam moment normalization uncertainty is $\pm 0.7\%$ [20] for the $^{119}\text{Sn}(\vec{d}, t) T_{20}$ data at 4.9 and 6.0 MeV, and $\pm 2\%$ [18] for the old data and the rest of the new data.

V. RESULTS

In order to obtain a final value for η_t , we have to decide how to weight the individual results. The procedure we use is to calculate the overall uncertainty

$$\Delta\eta_t = \left[(\Delta\eta_t^S)^2 + (\Delta\eta_t^C)^2 + (\Delta\eta_t^N)^2 \right]^{1/2} \quad (8)$$

for each result and then take the weighting factors to be inversely proportional to the square of these overall uncertainties. While other weighting procedures could have been adopted, we feel that the method described leads to the most reasonable distribution of weights for our data set. To take the large scatter of some of the measurements (particularly the $^{147}\text{Sm} T_{20}$ measurements) into account, we have multiplied $\Delta\eta_t^S$ by $\sqrt{\chi_r^2}$ for those individual results for which $\sqrt{\chi_r^2}$ is greater than 1. This gives these possibly less reliable measurements a smaller weight in determining the final result. The weights obtained in this way are given in Table II. The result of combining the individual η_t values using these weights is $\eta_t = -0.0431$. We point out that if the measurements of Ref. [11] were included with our measurements in this

weighting process, the Ref. [11] measurements would receive about one-third of the total weight.

To obtain a value for the uncertainty in η_t , we need to take into account the fact that the uncertainties of the individual η_t determinations are partially correlated. The statistical errors $\Delta\eta_t^S$ are completely uncorrelated, and the beam polarization normalization errors $\Delta\eta_t^N$ are uncorrelated except for measurements of the same analyzing power at the same energy. It is not known, however, how the errors in the calculation, $\Delta\eta_t^C$, are correlated. If an optical model parameter used in one calculation is incorrect, that parameter may or may not be incorrect for other energies or target nuclei. Also, different reactions have different sensitivities to the individual parameters. We have chosen to compute the uncertainty under the assumption that the calculational uncertainties are completely correlated (this is the worst-case assumption), while the statistical uncertainties are uncorrelated and the beam polarization normalization uncertainties are correlated to the extent mentioned above. When this is done, the result is $\Delta\eta_t = 0.0025$. The reduced χ^2 for the set is 1.45 (corresponding to a confidence level of 13%), taking into account only the statistical errors. The final result of $\eta_t = -0.0431 \pm 0.0025$ is shown by the solid line and the dashed error bands in Fig. 6 along with the individual determinations of η_t .

To check our estimate of $\Delta\eta_t^C$, we can look at the results for the higher-energy ^{119}Sn data. As pointed out earlier, we do not expect these results to be accurate, nor do we expect the calculation of $\Delta\eta_t^C$ as described above to be as meaningful as at sub-Coulomb energies. However, looking at these higher-energy data can give us a check on our error estimates. With the uncertainties

(given in Table III) calculated in the same way as for the rest of the data, the higher-energy results lie within 1.5σ of the weighted mean of the sub-Coulomb data. This indicates that the method of error estimation is probably reasonable.

VI. CONCLUSION

By comparing sub-Coulomb (\vec{d}, t) tensor analyzing powers to full finite-range DWBA calculations including tensor potentials, we have obtained a value for η_t of -0.0431 ± 0.0025 . The quoted uncertainty includes statistical errors, errors in the theoretical calculations, and beam moment normalization errors. This value is in good agreement with the recent experimental determinations of Refs. [8, 11], and with the theoretical predictions of Refs. [3–5]. We believe that our result is the most accurate experimental determination of η_t to date because of the large data set that was used, the low energy at which the measurements were made, and the care with which the uncertainty was estimated.

ACKNOWLEDGMENTS

We would like to thank Dr. Y. Tagishi for providing numerical values of d - ^{208}Pb elastic scattering data. We also thank the other members of the Wisconsin nuclear physics group for their help in data acquisition. This work was supported in part by National Science Foundation Grant No. PHY-9019983.

-
- [1] L. D. Knutson, P. C. Colby, and B. P. Hichwa, *Phys. Rev. C* **24**, 411 (1981).
 - [2] S. Sen and L. D. Knutson, *Phys. Rev. C* **26**, 257 (1982).
 - [3] S. Ishikawa and T. Sasakawa, *Phys. Rev. Lett.* **56**, 317 (1986).
 - [4] J. L. Friar, B. F. Gibson, D. R. Lehman, and G. L. Payne, *Phys. Rev. C* **37**, 2859 (1988).
 - [5] T. Frederico, S. K. Adhikari, and M. S. Hussein, *Phys. Rev. C* **37**, 364 (1988).
 - [6] I. Borbély, V. König, W. Grüebler, B. Jenny, and P. A. Schmelzbach, *Nucl. Phys.* **A351**, 107 (1981).
 - [7] I. Borbély, W. Grüebler, V. König, P. A. Schmelzbach, and B. Jenny, *Phys. Lett.* **109B**, 262 (1982).
 - [8] B. Vuaridel, W. Grüebler, V. König, K. Elsener, P. A. Schmelzbach, M. Bittcher, D. Singy, I. Borbély, M. Bruno, F. Cannata, and M. D'Agostino, *Nucl. Phys.* **A499**, 429 (1989).
 - [9] O. Karban and J. A. Tostevin, *Phys. Lett.* **103B**, 259 (1981).
 - [10] C. M. Bhat, T. B. Clegg, H. J. Karwowski, and E. J. Ludwig, *Phys. Rev. C* **37**, 1358 (1988).
 - [11] R. K. Das, T. B. Clegg, H. J. Karwowski, and E. J. Ludwig, *Phys. Rev. Lett.* **68**, 1112 (1992).
 - [12] J. T. Londergan, C. E. Price, and E. J. Stephenson, *Phys. Lett.* **120B**, 270 (1983).
 - [13] D. D. Pun Casavant, J. G. Sowinski, and L. D. Knutson, *Phys. Lett.* **154B**, 6 (1985).
 - [14] R. C. Johnson and F. D. Santos, *Part. Nucl.* **2**, 285 (1971).
 - [15] W. W. Daehnick, J. D. Childs, and Z. Vrcelj, *Phys. Rev. C* **21**, 2253 (1980). Potential L from Table III was used.
 - [16] E. A. George and L. D. Knutson, *Phys. Rev. Lett.* **69**, 2447 (1992).
 - [17] W. Haeberli, M. D. Barker, C. A. Gossett, D. G. Mavis, P. A. Quin, J. Sowinski, T. Wise, and H. F. Glavish, *Nucl. Instrum. Methods* **196**, 319 (1982).
 - [18] K. Stephenson and W. Haeberli, *Nucl. Instrum. Methods* **169**, 483 (1980).
 - [19] Madison Convention, in *Polarization Phenomena in Nuclear Reactions* (University of Wisconsin Press, Madison, 1971), p. xxv.
 - [20] N. L. Rodning, Ph.D. thesis, University of Wisconsin, 1986.
 - [21] L. D. Knutson, *Ann. Phys. (N.Y.)* **106**, 1 (1977).
 - [22] C. M. Bhat, J. E. Bowsher, T. B. Clegg, H. J. Karwowski, E. J. Ludwig, and B. A. Brown, *Phys. Rev. C* **38**, 1537 (1988).
 - [23] M. H. Macfarlane and S. C. Pieper, ANL-76-11 Rev. 1 (unpublished), modified by R. P. Goddard (February, 1980).

- [24] F. D. Becchetti and G. W. Greenlees, in *Polarization Phenomena in Nuclear Reactions* (University of Wisconsin Press, Madison, 1971), p. 682.
- [25] P. W. Keaton and D. D. Armstrong, *Phys. Rev. C* **8**, 1692 (1973).
- [26] T. Murayama, Y. Tagishi, T. Sakai, M. Tomizawa, H. Nishikawa, and S. Seki, *Nucl. Phys.* **A486**, 261 (1988).
- [27] L. D. Knutson and W. Haeberli, *Phys. Rev. C* **12**, 1469 (1975).
- [28] J. E. Kammeraad and L. D. Knutson, *Nucl. Phys.* **A435**, 502 (1985).
- [29] N. L. Rodning and L. D. Knutson, *Phys. Rev. C* **41**, 898 (1990).
- [30] M. H. Lopes, J. A. Tostevin, and R. C. Johnson, *Phys. Rev. C* **28**, 1779 (1983).
- [31] J. A. Tostevin, *Nucl. Phys.* **A466**, 349 (1987); J. A. Tostevin and R. C. Johnson, *Phys. Lett.* **124B**, 135 (1983).
- [32] P. W. Woods, R. Chapman, J. N. Mo, P. Skensved, and J. A. Kuehner, *Phys. Lett.* **116B**, 320 (1982).
- [33] J. M. Lohr, Ph.D. thesis, University of Wisconsin, 1972.
- [34] J. M. Lohr and W. Haeberli, *Nucl. Phys.* **A232**, 381 (1974). The potential of Eqs. (1)–(3) was used, with $a_0 = 0.86$.
- [35] J. Bojowald, H. Machner, H. Nann, W. Oelert, M. Rogge, and P. Turek, *Phys. Rev. C* **38**, 1153 (1988). The potential of Eq. (6) was used.
- [36] G. Perrin, Nguyen Van Sen, J. Arvieux, R. Darves-Blanc, J. L. Durand, A. Fiore, J. C. Gondrand, F. Merchez, and C. Perrin, *Nucl. Phys.* **A282**, 221 (1977). The potential of Table IV was used.
- [37] R. A. Hardekopf, R. F. Haglund, Jr., G. G. Ohlsen, W. J. Thompson, and L. R. Veaser, *Phys. Rev. C* **21**, 906 (1980). The potentials of Table II were used. For ^{118}Sn , the potential for ^{116}Sn was used; for ^{147}Sm , the potential for ^{140}Ce was used; for ^{207}Pb , the potential for ^{208}Pb was used.
- [38] E. R. Flynn, D. D. Armstrong, J. G. Beery, and A. G. Blair, *Phys. Rev.* **182**, 1113 (1969). The potential of Table II was used, and a spin-orbit potential with $V_{\text{SO}} = 6$ MeV, $r_{\text{SO}} = 1.1$ fm, and $a_{\text{SO}} = 0.65$ fm was included. For ^{147}Sm , the potential for ^{124}Sn was used; for ^{207}Pb , the potential for ^{208}Pb was used.
- [39] T. Sasakawa and T. Sawada, *Phys. Rev. C* **19**, 203 (1979).